Supplementary Notes

Summary of downloadable files

To ensure full transparency, reproducibility, and reuse of the database developed and compiled in this study, we list the datasets available in the zenodo repository (https://doi.org/10.5281/zenodo.21130189) in six thematic Supplementary Notes (SN1-SN6). Each of the following Supplementary Notes is associated with a *Supplementary Folder (SF)* in the repository. The Notes contain a brief description of the original, digitized, harmonized or derived datasets used in the construction and validation of the 3D crustal framework (**Table 3** of main text). The tables below provide a detailed inventory of all downloadable files, including their scientific purpose, associated figures in the main manuscript and file format. Together, these datasets constitute the complete digital archive supporting the results presented in this work and are intended to facilitate independent verification, future applications, and further developments of the proposed modelling framework.

Supplementary Note 1

Seismic tomography datasets

To facilitate reproducibility and future applications of the proposed framework, we provide both the original seismic tomography dataset and the resampled velocity model employed throughout this study (**Figure S1**).

The *Supplementary Folder SF1* contains the following files:

- **Im25.csv**
  Original 3D P-wave velocity tomography dataset published by Magnoni et al. (2022) and used as the primary seismic input for this study.
- **Tomo_resampled_5km_5km_1km_to50km.mat**
  MATLAB file containing the resampled 3D P-wave velocity model.
- **Tomo_resampled_5km_5km_1km_to50km.txt**
  ASCII version of the resampled model provided as four columns: 'X (m)   Y (m)   Z (m)   Vp (m/s)'
- **Header_file_Tomo_resampled.txt**
  Summary of the grid characteristics.

The original tomography was interpolated onto a regular Cartesian grid with a horizontal spacing of 5 km × 5 km and a vertical spacing of 1 km, extending from the surface down to 50 km depth. Linear interpolation was applied and the resulting model was clipped using the study-area buffer. The final resampled volume contains 211308 valid cell nodes distributed within the modelled domain. The resampled model represents the reference seismic dataset used in the workflow and was employed to extract the P-wave velocity isosurfaces associated with the main crustal interfaces discussed in the manuscript.

Table S1: Inventory of datasets included in Supplementary Folder 1.

Data file	Reference figure/table	Description	Format	SF
Im25.csv	Fig. S1	Original seismic tomography dataset.	.csv	SF1
Tomo.mat	Fig. S1	Processed tomography dataset used as input.	.mat	SF1
Tomo_resampled_5km_5km_1km_to50km .mat	Fig. S1	Resampled tomography model.	.mat	SF1
Tomo_resampled_5km_5km_1km_to50km .txt	Fig. S1	ASCII file of the resampled tomography model.	.txt	SF1
Header_file_Tomo_resampled.txt	Fig. S1	Metadata.	.txt	SF1

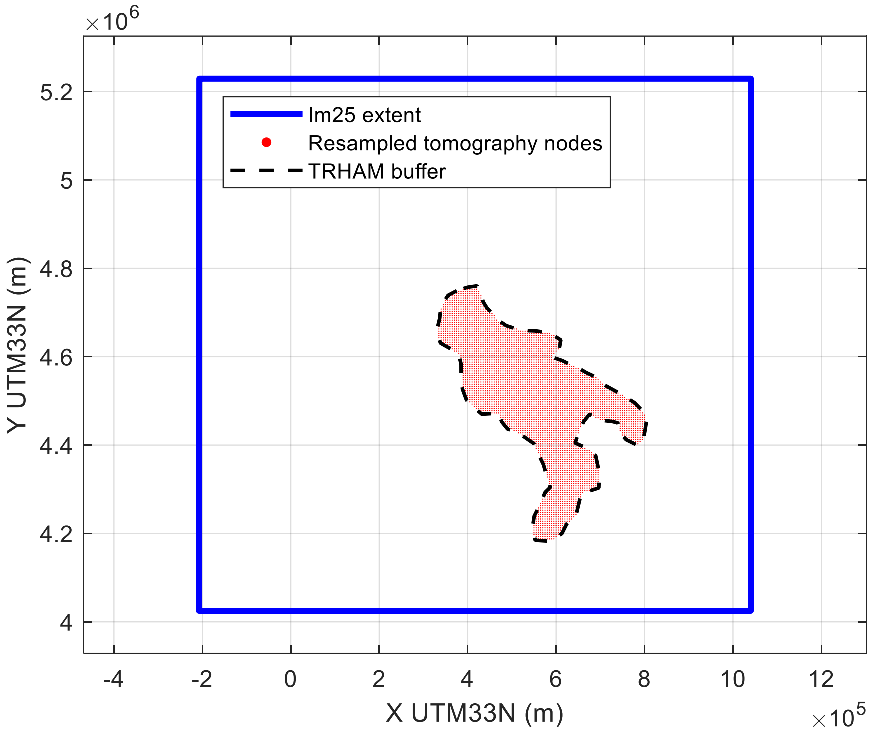

Figure S1: Spatial coverage of the original and resampled tomography datasets used in the study area. The dashed black line indicates the boundary of the study area. The blue polygon outlines the spatial extent of the original tomographic model of Magnoni et al. (2022) (*Im25*). Red dots represent the nodes of the resampled tomographic model (5 km × 5 km × 1 km resolution) extracted within the buffer and subsequently used for the construction of the 3D velocity model down to 50 km depth.

Supplementary Note 2

Main regional structural features

In the *Supplementary Folder SF2*, we provide the three structural traces shown in **Figure 3** of the main text (labelled [1], [2], and [3] in red). Each file contains the Easting and Northing coordinates (UTM Zone 33N) of the mapped structural feature, allowing its direct visualization and integration within GIS or other geospatial software.

Table S2: Inventory of datasets included in Supplementary Folder 2.

Data file	Reference figure/table	Description	Format	SF
Feature1_outcropping.dat	Fig. 3	Digitized trace of outcropping structural Feature 1.	.dat	SF2
Feature2_buried.dat	Fig. 3	Digitized trace of buried structural Feature 2.	.dat	SF2
Feature3_outcropping.dat	Fig. 3	Digitized trace of outcropping structural Feature 3.	.dat	SF2

Supplementary Note 3

Constraints on Moho *p-wave* velocities

The Moho discontinuity cannot be sharply resolved using the tomographic model of Magnoni et al. (2022), owing to the limited vertical resolution at depths greater than approximately 45 km. To improve these constraints, we evaluated P-wave velocities at Moho depths independently inferred from Receiver Function (RF) analyses by Spada et al. (2013) and compared them with the corresponding velocities extracted from the tomography of Magnoni et al. (2022). From the RF dataset, we retained only stations characterized by an uncertainty ≤10 km, resulting in 31 reliable estimates out of the 59 stations reported by Spada et al. (2013).

In the Adriatic domain, where RF data place the Moho at depths of approximately 30–32 km, the tomographic P-wave velocities at these depths are ~7.5 km s^{-1}. These values are consistent with global estimates for the onset of upper-mantle materials and with literature constraints on typical Moho Vp values (e.g., Diehl et al., 2009; Di Stefano et al., 20011; Di Stefano and Ciaccio, 2014). In contrast, the Tyrrhenian side, characterized by a thinner crust and higher thermal gradients, exhibits a shallower Moho (~20–25 km) associated with lower velocities (~7.1 km s^{-1}), reflecting both crustal thinning beneath the Tyrrhenian hinterland and elevated lithospheric temperatures.

As detailed in the main text, we further assessed the consistency of the Spada et al. (2013) Moho surface by comparing it with the lower boundary of a gravimetric model obtained from the inversion of regional Bouguer anomalies, specifically the crystalline basement bottom surface derived by Kelemework et al. (2021). Across most of the study region, the depth difference between the two surfaces is within 1-2 km, indicating strong agreement between independent datasets and methodologies. Larger discrepancies (2–3 km) occur locally in tectonically complex areas or regions characterized by sparse seismic coverage. These deviations remain within the expected resolution limits of both approaches, considering the uncertainty of the RF-derived Moho estimates (3–10 km; Spada et al., 2013) and the sensitivity and parameterization range of the gravimetric inversion (2–5 km; Kelemework et al., 2021).

To ensure transparency and reproducibility of the analyses presented in this study, *Supplementary Folder SF4* includes the original Moho surfaces published by Spada et al. (2013), provided as two separate grid files (*.grd*) corresponding to the Adriatic and Tyrrhenian domains, together with the complete Receiver Function (RF) dataset used in their study. For direct comparison, we also provide the crystalline basement bottom surface derived by Kelemework et al. (2021), available in both ASCII (*.dat*) and Surfer grid (*.grd*) formats.

We further provide the unified Moho surface (*.dat*) adopted in this work and used throughout the integrated 3D crustal model (e.g., **Fig. 7f** of the main text). This dataset represents the harmonized Moho interface obtained by integrating the original Adriatic and Tyrrhenian RF-derived surfaces with additional independent geophysical constraints.

In addition, we provide the spreadsheet used for the station-by-station comparison between the discontinuity depths inferred from the Receiver Function analysis of Spada et al. (2013) and the corresponding seismic velocities extracted from the tomographic model of Magnoni et al. (2022). The workbook includes the original RF-derived depths (Mo1, Mo2, and InCr), together with their associated ±1σ uncertainty bounds, as well as the corresponding P-wave and S-wave velocities extracted from the tomography at the same locations and depths. This dataset therefore provides a direct comparison between the RF-derived interfaces and the raw tomographic model and forms the basis of the analysis presented in this Supplementary Note, including the estimation of the average P-wave velocities associated with the Adriatic and Tyrrhenian Moho domains.

Table S3: Inventory of datasets included in Supplementary Folder 3.

Data file	Reference figure/table	Description	Format	SF
Moho_Map_AlpsMediCentral-Spadaetal2013_Adriatic_NEG_meter.grd	Fig. 8f	Original Adriatic Moho depth surface derived from Receiver Function (RF) analyses by Spada et al. (2013). Grid values represent Moho depth below sea level (negative values, metres).	.grd	SF3
Moho_Map_AlpsMediCentral-Spadaetal2013_Tyrrhenian_NEG_meter.grd	Fig. 8f	Original Tyrrhenian Moho depth surface derived from Receiver Function analyses by Spada et al. (2013). Grid values represent Moho depth below sea level (negative values, metres).	.grd	SF3
Moho_Spada_2013.txt	Fig. 8f	Unified Moho surface adopted in the TRHAM framework	.txt	SF3
RF_Spada_2013.txt	Fig. 8f	Complete RF station dataset from Spada et al. (2013).	.txt	SF3
Kelemework_etal_2021_crystallineBOTTOM.grd	Fig. 8f	bottom surface of Crystalline basement from Kelemework et al. (2021).	.grd	SF3
Kelemework_etal_2021_crystallineBOTTOM.dat	Fig. 8f	ASCII file of bottom surface of the crystalline basement.	.dat	SF3
Moho_depth_vpvs_StudyArea.xlsx	Fig. 8f	Station-by-station comparison between RF-derived discontinuities and tomography-derived Vp/Vs values.	.xlsx	SF3

Supplementary Note 4

Modelled intra-crustal transition surfaces

To facilitate reproducibility and reuse of the 3D crustal model, the *Supplementary Folder 4* contains the digital surfaces, shown in **Figure 8** of the main text. Geological interfaces are provided as both Surfer grid files (*.grd*) and ASCII point files (*.dat*) containing Easting, Northing, and depth coordinates. The topographic surface (DEM) is provided separately in its original *.dem* format.

The supplied surfaces in *Supplementary Folder SF5*, include:

- the Digital Elevation Model (DEM) of the study area (UTM Zone 33N);
- the top of the carbonate platform;
- the top of the siliciclastic succession (sandstones);
- the top of the crystalline basement (gneissic domain);
- the top of the gabbroic lower crust;
- the Moho surface adopted in the integrated crustal model.

Although the Moho geometry and its derivation are described in *Supplementary Note* 4, the corresponding surface is also included here to provide the complete set of interfaces used to construct the geological framework shown in **Figure 8** (main text). All datasets are referred to the UTM Zone 33N coordinate system and can be directly imported into GIS, Surfer, or any other 3D modeling software.

Table S4: Inventory of datasets included in Supplementary Folder 4.

Data file	Reference figure/table	Description	Format	SF
StudyArea_DEM_UTM33N.dem	Fig. 8	DEM derived from Tarquini et al. (2023).	.dem	SF4
DEM_SudItalia_500m_UTM33N.grd	Fig. 8	Regional DEM resampled to 500 m.	.grd	SF4
Moho_panelF_SpadaEtAl2013.grd	Fig. 8	Used Moho surface.	.grd	SF4
Moho_panelF_SpadaEtAl2013.dat	Fig. 8	ASCII file of final Moho surface.	.dat	SF4
Top_gabbro.grd	Fig. 8	Top gabbro surface.	.grd	SF4
Top_gabbro.dat	Fig. 8	ASCII file top gabbro surface.	.dat	SF4
Top_gneiss.grd	Fig. 8	Top gneiss surface.	.grd	SF4
Top_gneiss.dat	Fig. 8	ASCII file top gneiss surface.	.dat	SF4
Top_limestones.grd	Fig. 8	Top limestone surface.	.grd	SF4
Top_limestones.dat	Fig. 8	ASCII top limestone surface.	.dat	SF4
Top_sandstones.grd	Fig. 8	Top sandstone surface.	.grd	SN4
Top_sandstones.dat	Fig. 8	ASCII top sandstone surface.	.dat	SN4

Supplementary Note 5

Pressure-temperature corrected *p-wave* velocities

To complement the main petrophysical modeling, in **Figure S2** we provide additional velocity-depth profiles for lithologies not highlighted in bold in **Table 2** of main text, offering pressure-temperature corrected data for broader application. Users may select the most appropriate lithology based on the specific goals and geological context of their study.

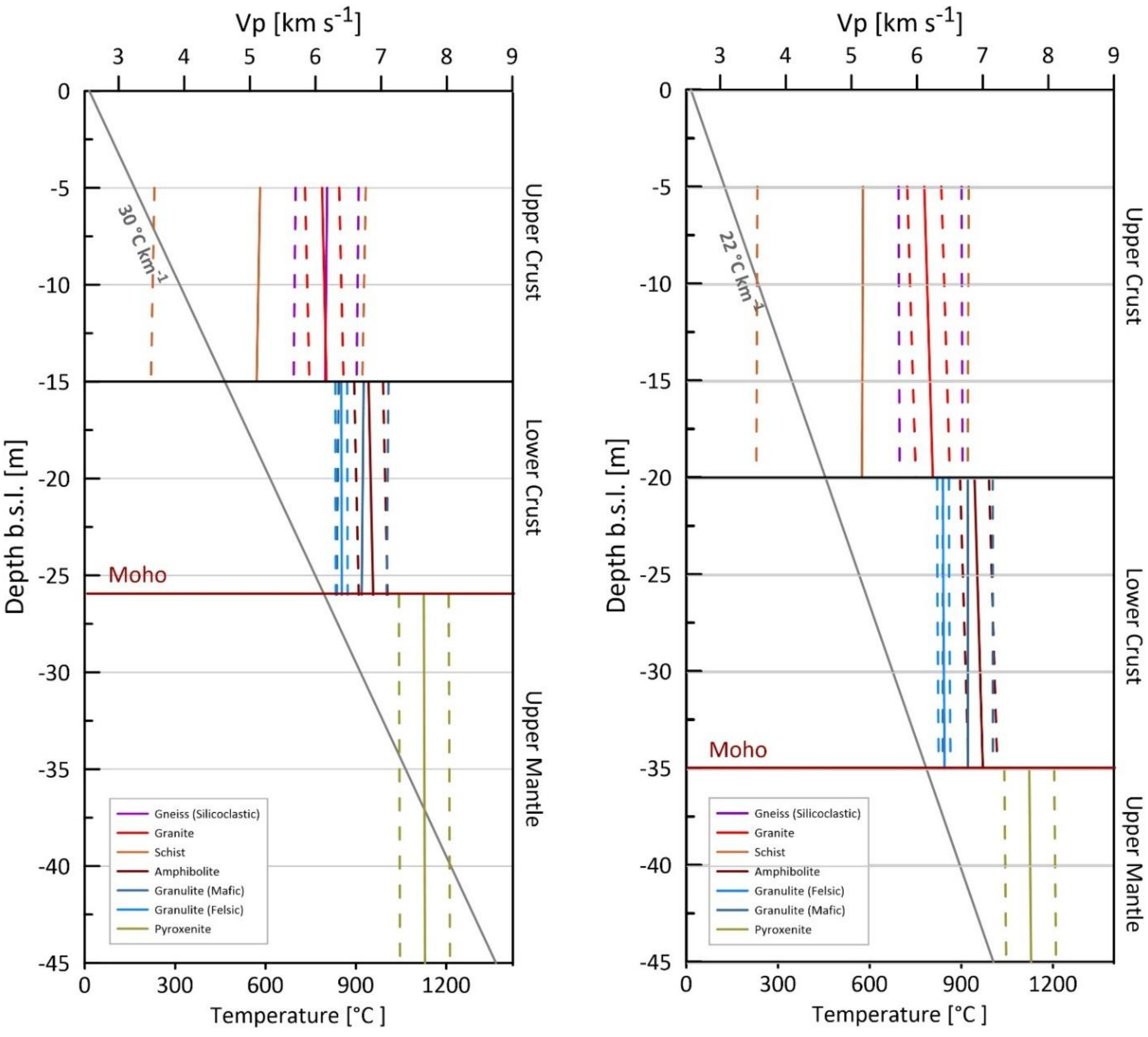

Figure S2: Velocity-depth profiles constructed using data from this work for lithologies not highlighted in bold in **Table 2**. The average P-wave velocity (continuous lines) and associated ±1σ uncertainty (dashed lines) are shown. The two thermal scenarios represent (a) a thinned crust (26 km) with a hot geotherm (grey line, 30 °C/km) and (b) a thick crust (35 km) with a cold geotherm (grey line, 22 °C/km). Although not included in the 3D crustal modeling presented in **Figure 9** (main text), these additional lithologies are corrected for pressure and temperature conditions and provided as reference profiles.

In addition, the *Supplementary Folder SF5* contains the original datasets used to generate **Figure 5** of the main text, including the pressure- and temperature-dependent correction data for the considered lithologies, thus ensuring full reproducibility of the petrophysical workflow.

Table S5: Inventory of datasets included in Supplementary Folder 5.

Data file	Reference figure/table	Description	Format	SF
Table_2.xlsx	Table 2	Pressure- and temperature-corrected P-wave velocities adopted in the workflow.	.xlsx	SF5
amphibolite_PTS_T_panelB.txt	Fig. 5	Temperature-dependent velocity correction curve for amphibolite.	.txt	SF5
gabbro_PTS_P_panelA.txt	Fig. 5	Pressure-dependent velocity correction curve for gabbro.	.txt	SF5
gneiss_PTS_P_panelA.txt	Fig. 5	Pressure-dependent velocity correction curve for gneiss.	.txt	SF5
gneiss_PTS_T_panelB.txt	Fig. 5	Temperature-dependent velocity correction curve for gneiss.	.txt	SF5
granite_PTS_T_panelB.txt	Fig. 5	Temperature-dependent velocity correction curve for granite.	.txt	SF5
granulite_PTS_P_panelA.txt	Fig. 5	Pressure-dependent velocity correction curve for granulite.	.txt	SF5
granulite_PTS_T_panelB.txt	Fig. 5	Temperature-dependent velocity correction curve for granulite.	.txt	SF5
peridotite_PTS_P_panelA.txt	Fig. 5	Pressure-dependent velocity correction curve for peridotite.	.txt	SF5
Table_references.xlsx	Fig. 5	Bibliographic references used to derive correction datasets.	.xlsx	SF5

Supplementary Note 6

Reference surfaces and borehole data used for model validation

To facilitate independent verification of the validation procedures presented in the main text, the *Supplementary Folder SF6* includes the reference geological surfaces and borehole datasets used in **Figures 10-12**.

The folder *"Surfaces and VIDEPI wells Figure 9"* contains the digital surfaces compiled from the studies of Vezzani et al. (2010), Kelemework et al. (2021), and Trumpy et al. (2023), which were used as independent constraints for the validation of the model-derived discontinuities. These datasets are provided in both grid (*.grd*) and ASCII (*.dat*) formats. The crystalline basement bottom surface derived from Kelemework et al. (2021) is also included. Although this surface extends well beyond the study area and covers a large portion of the Italian mainland and offshore regions, it is provided because it is used as an independent reference in the profile-based comparisons shown in **Figure 11**. In addition, the spreadsheet TOP_apula_VIDEPIwells.xlsx contains the subset of VIDEPI boreholes intersecting the top of the Apulian carbonate platform within the study area, excluding the Calabria region as discussed in the main text. For each well, the file reports the coordinate and depth information used in the validation analyses presented in **Figures 11** and **12**.

The folder *"VIDEPI wells along profiles in **Figure 11**"* contains the borehole data extracted along the five regional profiles shown in **Figure 10** and subsequently analyzed in the cross-sections of **Figure 11**. These datasets are provided in ASCII (*.txt*) format and include the wells intersecting the top of the Apulian carbonate platform along each profile.

Table S6: Inventory of datasets included in Supplementary Folder 6.

Data file	Reference figure/table	Description	Format	SF
Vezzani_etal_2010.grd	Fig. 10	Digitized geological surface derived from Vezzani et al. (2010).	.grd	SF6
Vezzani_etal_2010.dat	Fig. 10	ASCII file of Vezzani surface.	.dat	SF6
Trumpy_etal_2023.grd	Fig. 10	Surface digitized from the published map of Trumpy et al. 2023	.grd	SF6
Trumpy_etal_2023.dat	Fig. 10	ASCII file of digitized Trumpy surface.	.dat	SF6
Kelemework_etal_2021_crystallineBOTTOM.grd	Fig. 12	Bottom surface of magnetic crystalline basement derived from Kelemework et al. (2021).	.grd	SF6
Kelemework_etal_2021_crystallineBOTTOM.dat	Fig. 12	ASCII file of bottom surface of magnetic crystalline basement derived from Kelemework et al. (2021).	.dat	SF6
Kelemework_etal_2021_crystallineTOP.grd	Fig. 12	Top surface of magnetic crystalline basement derived from Kelemework et al. (2021).	.grd	SF6

Kelemework_etal_2021_crystallineTOP.dat	Fig. 12	ASCII file of top surface of magnetic crystalline basement derived from Kelemework et al. (2021).	.dat	SF6
TOP_apula_VIDEPIwells.xlsx	Fig. 10	Top Apulia Platform depths from VIDEPI wells.	.xlsx	SF6
PROFILE_1.txt	Fig. 11	Constraints projected onto profile 1.	.txt	SF6
PROFILE_2.txt	Fig. 11	Constraints projected onto profile 2.	.txt	SF6
PROFILE_3.txt	Fig. 11	Constraints projected onto profile 3.	.txt	SF6
PROFILE_4.txt	Fig. 11	Constraints projected onto profile 4.	.txt	SF6
PROFILE_5.txt	Fig. 11	Constraints projected onto profile 5.	.txt	SF6

References

Di Stefano, R., Bianchi, I., Ciaccio, M. G., Carrara, G., and Kissling, E.: Three-dimensional Moho topography in Italy: New constraints from receiver functions and controlled source seismology, *Geochem. Geophys. Geosyst.*, **12**, Q09006, https://doi.org/10.1029/2011GC003649, 2011.

Di Stefano, R. and Ciaccio, M. G.: The lithosphere and asthenosphere system in Italy as inferred from the Vp and Vs 3D velocity model and Moho map, *J. Geodyn.*, **82**, 16–25, 2014.

Diehl, T., Husen, S., Kissling, E., and Deichmann, N.: High-resolution 3-D P-wave model of the Alpine crust, *Geophys. J. Int.*, **179**, 1133–1147, https://doi.org/10.1111/j.1365-246X.2009.04331.x, 2009.

Kelemework, Y., Milano, M., La Manna, M., et al.: Crustal structure in the Campanian region (Southern Apennines, Italy) from potential field modelling, *Sci. Rep.*, **11**, 14510, https://doi.org/10.1038/s41598-021-93945-8, 2021.

Magnoni, F., Casarotti, E., Komatitsch, D., Di Stefano, R., Ciaccio, M. G., Tape, C., Melini, D., Michelini, A., Piersanti, A., and Tromp, J.: Adjoint tomography of the Italian lithosphere, *Commun. Earth Environ.*, **3**, 69, https://doi.org/10.1038/s43247-022-00397-7, 2022.

Spada, M., Bianchi, I., Kissling, E., Piana Agostinetti, N., and Wiemer, S.: Combining controlled-source seismology and receiver-function information to derive a 3-D Moho topography for Italy, *Geophys. J. Int.*, **194**, 1050–1068, https://doi.org/10.1093/gji/ggt148, 2013.

Tarquini, S., Isola, I., Favalli, M., Battistini, A., and Dotta, G.: *TINITALY, a digital elevation model of Italy with a 10 meters cell size (Version 1.1)* [data set], Istituto Nazionale di Geofisica e Vulcanologia (INGV), https://doi.org/10.13127/tinitaly/1.1, 2023.

Trumpy, E., Manzella, A., and Pertusati, P. C.: Regional scale surface of the top of the Variscan basement in the central sector of Italy, *J. Maps*, **19**, https://doi.org/10.1080/17445647.2023.2243981, 2023.

Vezzani, L., Festa, A., and Ghisetti, F. C.: *Geology and tectonic evolution of the Central-Southern Apennines, Italy*, *Geol. Soc. Am. Spec. Pap.*, **469**, https://doi.org/10.1130/2010.2469, 2010.